Materials Science and Engineering A 497 (2008) 426–431

Contents lists available at ScienceDirect

Materials Science and Engineering A

journal homepage: www.elsevier.com/locate/msea

Effect of of Yb, Cr and Zr additions on recrystallization and corrosion resistance of Al–Zn–Mg–Cu alloys

K.H. Chen[a,*], H.C. Fang[a], Z. Zhang[a], X. Chen[a], G. Liu[b]

[a] State Key Laboratory of Powder Metallurgy, Central South University, Changsha 410083, China
[b] State Key Laboratory for Mechanical Behavior of Materials, School of Material Science and Engineering, Xi'an Jiaotong University, Xi'an 710049, China

ARTICLE INFO

Article history:
Received 16 April 2008
Received in revised form 20 July 2008
Accepted 21 July 2008

Keywords:
Dispersoid
Ytterbium
Recrystallization
Intergranular corrosion
Exfoliation corrosion

ABSTRACT

The effect of complex additions of Yb, Cr and Zr on recrystallization and corrosion resistance of Al–Zn–Mg–Cu alloy has been investigated. By complex additions of Yb, Cr and Zr to Al–Zn–Mg–Cu alloy, 20–50 nm dispersoids were formed in Al matrix and identified by X-ray diffraction analysis and energy dispersive X-ray spectroscopy as Zn, Mg, Cu, Zr-containing $YbCr_2A1_{20}$ with cubic $CeCr_2Al_{20}$ crystal structure. The dispersoids remarkably inhibited the recrystallization of Al matrix, and a lot of low angle grain boundary of the Al–Zn–Mg–Cu alloy by complex additions of Zr, Cr and Yb investigated by electron back scattered diffraction was retained. Complex additions of Yb, Cr and Zr to Al–Zn–Mg–Cu alloy remarkably enhanced resistance to stress corrosion cracking (K_{ISCC}) from 9.8 to 17.0 MPa $m^{1/2}$, exfoliation corrosion from EB+ to EA and intergranular corrosion with the improved strength, fracture toughness and ductility.

1. Introduction

Ultra-high strength Al–Zn–Mg–Cu aluminum alloys with high strength, low density and good machining properties are widely used in the military and aerospace industries [1,2]. However, the recrystallization of Al matrix in the deformed alloy will happen during the high temperature solution treatment, and the subsequent recrystallized grain boundary with high angle grain boundary is preferentially eroded and cracked.

In order to improve recrystallization resistance of Al–Zn–Mg–Cu alloys, dispersoid-forming element such as Mn, Cr or Zr is often added. However, the recrystallization of Al–Zn–Mg–Cu alloy can not be inhibited completely by Mn, Cr or Zr addition [3,4], although Zr addition is more effective and widely used.

The addition of Sc to Al alloys is more effective to improve recrystallization resistance than Zr addition [5,6] due to the formation of a high density of Al_3Sc dispersoids. Complex addition of Sc and Zr to Al alloys can produce $Al_3(Sc,Zr)$ dispersoid which is more stable than Al_3Sc dispersoid, and further improve recrystallization resistance [7]. But Sc addition is too expensive to be extensively used in industry. The cheaper rare-earth element additions are being studied to replace Sc [8,9].

In previous research, present authors found that the 20–50 nm spherical dispersoids of $(Zr,Yb)Cr_2(Al,Zr)_{20}$ or Zr-containing $YbCr_2A1_{20}$ with $CeCr_2Al_{20}$ cubic crystal structure can be formed in Al matrix by complex additions of Yb, Cr and Zr to aluminum. Complex additions of Yb, Cr and Zr to Al–Zn–Mg–Cu alloy can obviously suppress the recrystallization of Al matrix, improve the fracture toughness, as well as remarkably enhance the stress corrosion resistance [10].

In the present research, the effect of complex additions of Yb, Cr and Zr to Al–Zn–Mg-Cu alloys on microstructure, mechanical properties and corrosion behaviors, including stress corrosion cracking (SCC), intergranular corrosion (IGC) and exfoliation corrosion (EXCO), were further investigated.

2. Materials and experimental

The nominal compositions of the alloys were shown in Table 1. High purity aluminum (99.9%), magnesium (99.9%) and zinc (99%), and Al–Zr, Al–Cu, Al–Cr and Al–Yb master alloys were smelted into the alloys. The smelting temperature was kept at 700–740 °C. The alloy melt was refined by adding 0.2–0.4 wt% C_2Cl_6, and cast into Ø 45 mm ingot in iron mould.

The cast ingots were treated at 465 °C for 24 h for homogenization, and extruded at 410–430 °C into plate of 13.5 mm × 10.2 mm section in 12.2 extrusion ratio. The extruded plates were held at 450 and 470 °C separately for 1 h, then kept at 480 °C for 2 h for stepped solution treatment, then were quenched in ambient temperature

* Corresponding author. Tel.: +86 731 8830714; fax: +86 731 8710855.
E-mail address: khchen@mail.csu.edu.cn (K.H. Chen).

0921-5093/$ – see front matter © 2008 Elsevier B.V. All rights reserved.
doi:10.1016/j.msea.2008.07.028

Table 1
Nominal compositions of three aluminum alloys (mass fraction, wt%)

Alloys	Zn	Mg	Cu	Zr	Cr	Yb	Al
AlZnMgCu–0.16Zr	8.6	2.5	2.2	0.16	–	–	Bal
AlZnMgCu–0.16Zr–0.2Cr–0.3Yb	8.6	2.5	2.2	0.16	0.20	0.30	Bal
AlZnMgCu–0.32Zr–0.4Cr–0.6Yb	8.6	2.5	2.2	0.32	0.40	0.60	Bal

water. The plates were tempered at 130 °C for 24 h for artificial T6 tempered.

The optical microscopy (OM) and transmission electron microscopy (TEM) were used to observe the microstructures of the tempered plates on a Polyver-Met optical microscope and TECNAI G^2 20 transmission electron microscope. The specimens for OM were electro-polished and anodized in HF and H_3BO_3 solution. Thin foils for TEM were prepared by twin jet-polishing in electrolyte solution of HNO_3 and methyl alcohol (1:3). Misorientation angles between grains were measured by using electron back scattered diffraction (EBSD) equipment of a HITACHI 3400 scanning electron microscope (SEM). Energy dispersive X-ray spectroscopy (EDXS) and SEM were performed to obtain the distribution and constitution of the dispersoids on a JEOL-6360LV SEM. X-ray diffraction analysis (XRD) was used to characterise the phases of samples on a D/max-2500 diffractometer with Cu Kα radiation.

Double cantilever beam (DCB) testing was carried out to study the stress corrosion cracking resistance according to GB12445.1-1990 [11]. The accelerated EXCO test was performed according to GB5455-1990 [12]. The accelerated IGC test was performed according to the IGC test standard of GB7998-1987 [13].

3. Results

3.1. Mechanical properties and electric conductivity

The tensile properties, fracture toughness and electric conductivity of the T6-tempered alloys are shown in Table 2. Complex additions of Cr, Yb and Zr can improve the strength, ductility, fracture toughness (K_{IC}) and electronic conductivity of ultra-high strength Al–Zn–Mg–Cu alloy.

3.2. Corrosion behaviors

3.2.1. Stress corrosion cracking

The effect of complex additions of Yb, Cr and Zr on the stress corrosion crack growth rate of T6-tempered Al–Zn–Mg–Cu alloy is shown in Fig. 1. AlZnMgCu–0.16Zr alloy has high growth rate of stress corrosion crack and the critical stress corrosion cracking intensity factor (K_{ISCC}) of 9.8 MPa $m^{1/2}$; Complex additions of Yb, Cr and Zr to Al–Zn–Mg–Cu alloy can remarkably decrease stress corrosion crack growth rate of the alloy and enhance K_{ISCC} from 9.8 to 17.0 MPa $m^{1/2}$.

3.2.2. Exfoliation corrosion

The effect of complex additions of Yb, Cr and Zr on the exfoliation corrosion of T6-tempered Al–Zn–Mg–Cu alloy is shown in Table 3. Compared to AlZnMgCu–0.16Zr alloy with exfoliation corrosion rank EB+ (notable layering and penetration into the metal) of after 48 h EXCO-testing, AlZnMgCu–0.16Zr–0.2Cr–0.3Yb alloy has higher exfoliation corrosion resistance, or exfoliation corrosion rank EA (tendency for undermining).

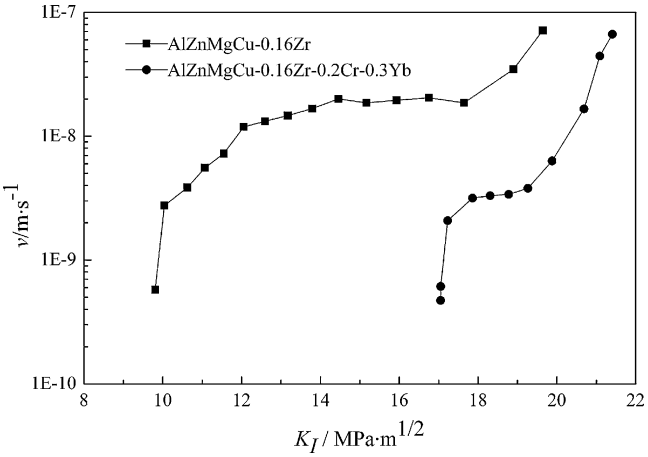

Fig. 1. Dependence of crack growth rate (v) of AlZnMgCu–0.16Zr and AlZnMgCu–0.16Zr–0.2Cr–0.3Yb alloys on crack tip stress intensity factor (K_I) in 3.5% NaCl solution.

Table 3
The ratings of EXCO after immersion into EXCO for different time

	Testing time (h)						
	1	2	4	8	12	24	48
Alloys							
AlZnMgCu–0.16Zr	N	P–	P	EA+	EA+	EB	EB+
AlZnMgCu–0.16Zr–0.2Cr–0.3Yb	N	N	P–	P	P+	EA–	EA

3.2.3. Intergranular corrosion

The effect of complex additions of Yb, Cr and Zr on the intergranular corrosion of T6-tempered Al–Zn–Mg–Cu alloy is shown in Fig. 2. The maximum intergranular corrosion depth of AlZnMgCu–0.16Zr and AlZnMgCu–0.16Zr–0.2Cr–0.3Yb alloys is 150.12 and 54.04 μm, respectively (Fig. 2) which indicates that complex additions of Yb, Cr and Zr to Al–Zn–Mg–Cu alloy can remarkably enhance the intergranular corrosion resistance.

3.3. Optical microstructure

The effect of complex additions of Yb, Cr and Zr on the optical microstructure of Al–Zn–Mg–Cu alloy is shown in Fig. 3. AlZnMgCu–0.16Zr alloy has partial recrystallized microstructure (Fig. 3a and b) and AlZnMgCu–0.16Zr–0.2Cr–0.3Yb alloy has fibrous unrecrystallized microstructure (Fig. 3c and d). That is, the recrystallization of Al matrix in Al–Zn–Mg–Cu alloy can not be inhibited completely by Zr additions only, and complex additions of Yb, Cr and Zr, compared to Zr addition, can more remarkably enhance the resistance to recrystallization of Al–Zn–Mg–Cu alloy.

3.4. EBSD

The typical grain boundary maps and misorientation angle histograms from SEM-EBSD measurements are shown in Fig. 4. There are a lot of low angle (less than 20°) grain boundary

Table 2
Mechanical properties and electric conductivity of T6-tempered alloys

Alloys	UTS (MPa)	YS (MPa)	El (%)	IACS (%)	K_{IC}(S-L) (MN/$m^{3/2}$)	K_{IC}(L-T) (MN/$m^{3/2}$)
AlZnMgCu–0.16Zr	709.7	683.6	8.9	32.1	21.6	32.8
AlZnMgCu–0.16Zr–0.2Cr–0.3Yb	747.1	725.2	9.3	34.5	29.3	42.5

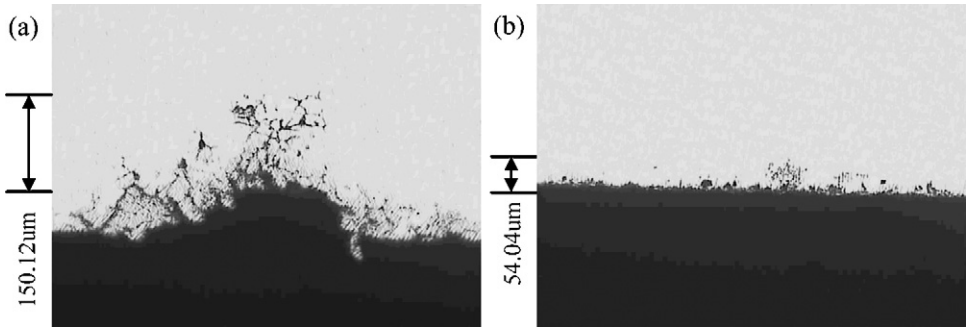

Fig. 2. Cross-section micrograph (perpendicular to the extrusion direction) of (a) AlZnMgCu–0.16Zr alloy and (b) AlZnMgCu–0.16Zr–0.2Cr–0.3Yb alloy after immersion in aqueous chloride-peroxide solution for 24 h.

in AlZnMgCu–0.16Zr–0.2Cr–0.3Yb alloy (Fig. 4c and d), whereas AlZnMgCu–0.16Zr has a high proportion of high angle (more than 30°) grain boundary (Fig. 4a and b).

3.5. X-ray powder diffraction analysis and SEM

The phases formed due to complex additions of Yb, Cr and Zr to Al–Zn–Mg–Cu alloy are shown in XRD pattern of Fig. 5. In the isothermal heat treated AlZnMgCu–0.32Zr–0.4Cr–0.6Yb alloy ingots, α(Al), $MgZn_2$ and $CeCr_2Al_{20}$ crystal structure (space group $Fd3m$, $Z=8$) [14] were identified by XRD. EDXS analysis showed that the dispersoids (in Fig. 6) precipitating in AlZnMgCu–0.16Zr–0.2Cr–0.3Yb and AlZnMgCu–0.32Zr–0.4Cr–0.6Yb alloys contained A1, Zn, Mg, Cu, Zr, Cr and Yb.

3.6. TEM

TEM micrographs of T6-tempered AlZnMgCu–0.16Zr–0.2Cr–0.3Yb alloy are shown in Fig. 7. 20–50 nm spherical dispersoids disperse in the grain and at the grain boundary (Fig. 7a). The chemical composition of both the dispersoids and α(Al) matrix were determined by EDXS, and summarized in Table 4.The spherical dispersoids contain Yb, Cr, Zr, Zn, Mg, Cu and Al according to EDXS analysis. Based on the XRD and EDXS,

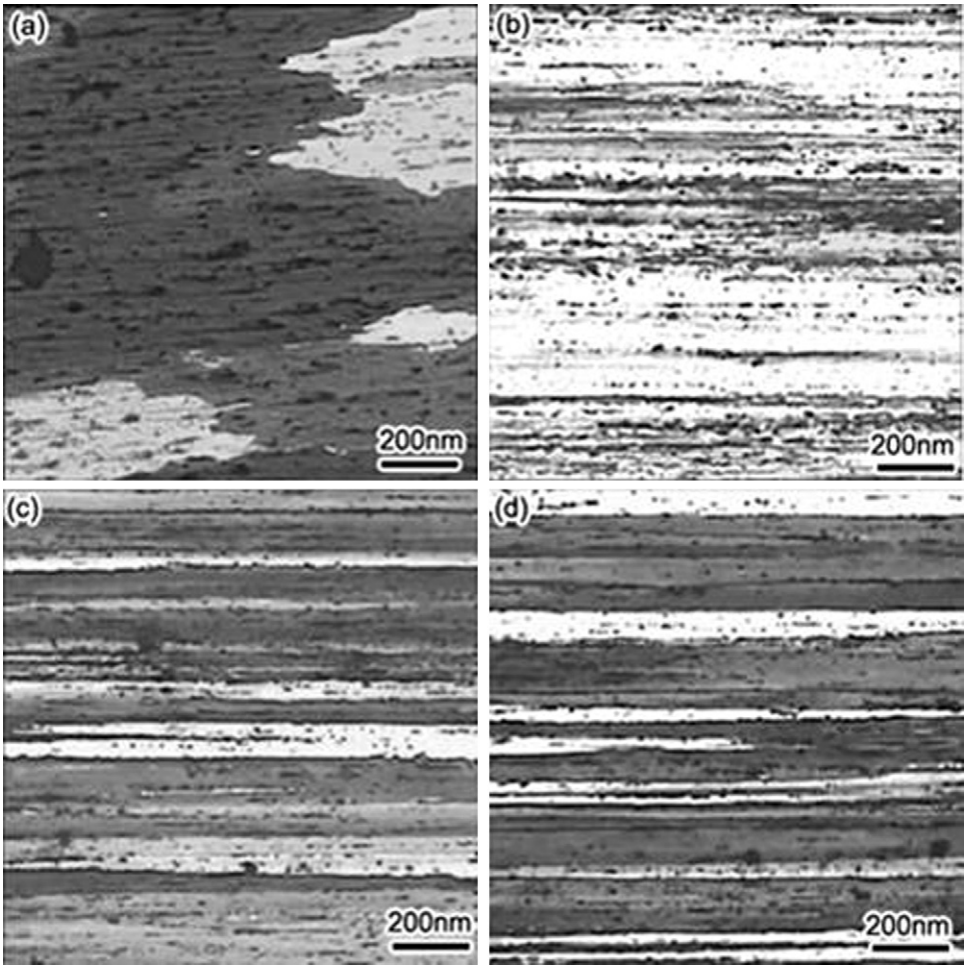

Fig. 3. Optical microstructures of AlZnMgCu–0.16Zr alloy: (a) L-T surface, (b) L-S surface, and AlZnMgCu–0.16Zr–0.2Cr–0.3Yb alloy: (c) L-T surface and (d) L-S surface.

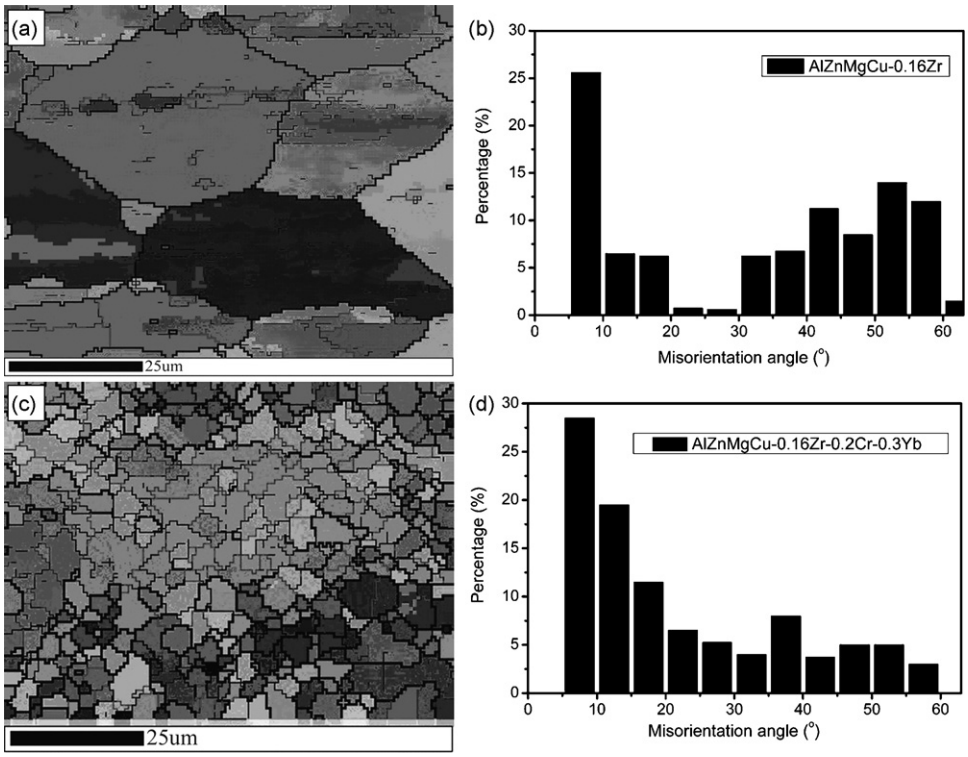

Fig. 4. AlZnMgCu–0.16Zr alloy: (a) grain boundary map, (b) misorientation distribution, and AlZnMgCu–0.16Zr–0.2Cr–0.3Yb alloy: (c) grain boundary map and (d) misorientation distribution.

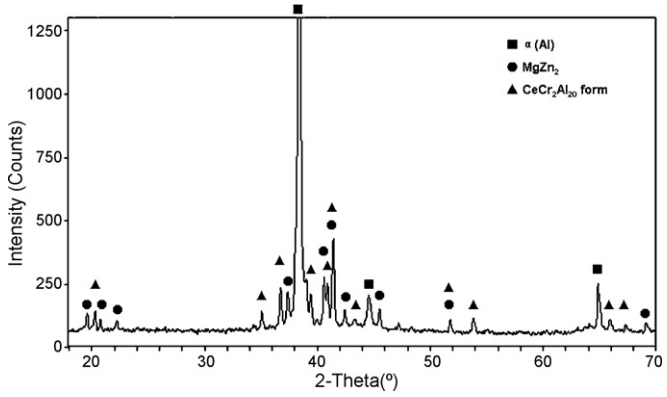

Fig. 5. XRD pattern of AlZnMgCu–0.32Zr–0.4Cr–0.6Yb alloy ingot isothermally heat treated for 168 h at 450 °C, composed of α(Al), $MgZn_2$ and $CeCr_2Al_{20}$ form phases.

it is suggested that Zr, Zn, Mg and Cu be dissolved in $YbCr_2Al_{20}$, substituting for Al and Yb atoms [15] and the dispersoid is close to $(Zr,Yb)Cr_2(Al, Zr, Zn, Mg, Cu)_{20}$.

The bright-field TEM micrographs of the T6-tempered alloys are showed in Fig. 8. In AlZnMgCu–0.16Zr alloy, Equilibrium η phase particles are distributed continuously on the grain boundaries (Fig. 8a), which leads to IGC, EXCO and SCC. In AlZnMgCu–0.16Zr–0.2Cr–0.3Yb alloy, equilibrium η phases are distributed more discontinuously on the grain boundaries (Fig. 8b), which is responsible for the improvement of the corrosion resistance.

4. Discussion

Al–Zn–Mg–Cu alloys of the T6 temper are susceptible to IGC, EXCO and SCC, which is highly related to η phase precipitation at the grain boundary. When the alloys are exposed to corrosion environment, η phase is anodic to Al matrix and will be dissolved preferentially. η phase particles are concentrated at grain boundary due to the energy difference between grain boundary and grain inte-

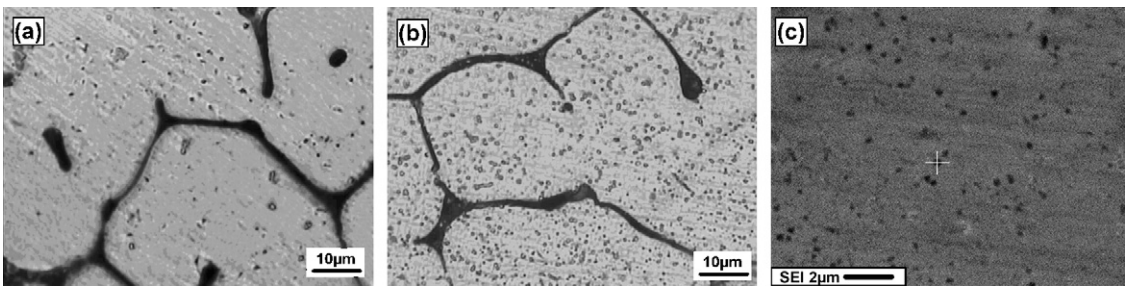

Fig. 6. Optical microscopy of dispersoids in (a) as-cast AlZnMgCu–0.16Zr–0.2Cr–0.3Yb alloy and (b) as-cast AlZnMgCu–0.32Zr–0.4Cr–0.6Yb alloy and (c) SEM of AlZnMgCu–0.32Zr–0.4Cr–0.6Yb alloy.

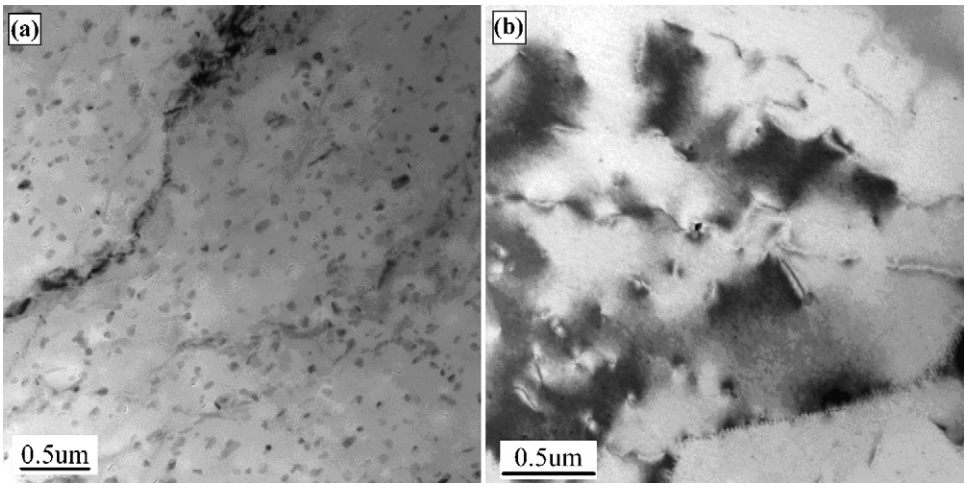

Fig. 7. TEM of T6-tempered AlZnMgCu–0.16Zr–0.2Cr–0.3Yb alloy.

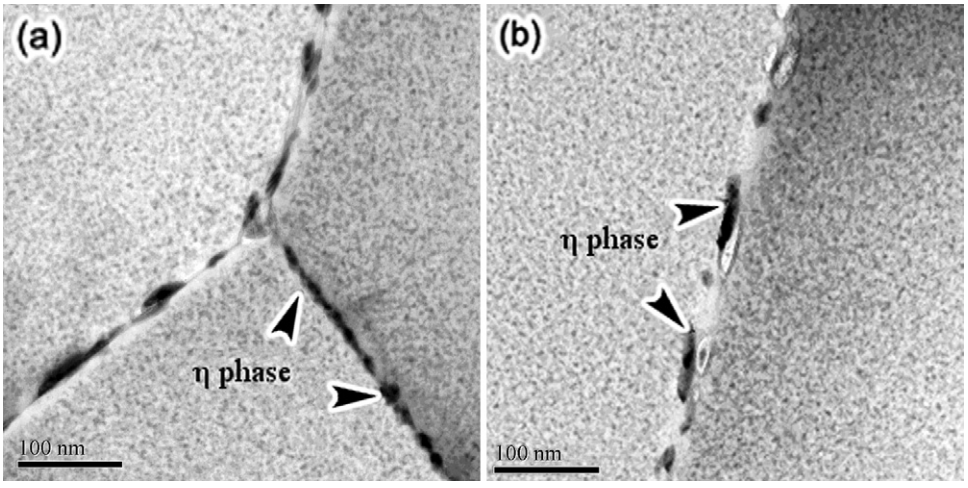

Fig. 8. TEM micrograph of alloys in T6 temper: in AlZnMgCu–0.16Zr alloy (a), continuous precipitate chains are found on the grain boundaries, and in AlZnMgCu–0.16Zr–0.2Cr–0.3Yb alloy (b), the discrete distribution of η phases are found on the grain boundaries.

Table 4
EDXS result for the dispersoid and α(Al) matrix in AlZnMgCu–0.16Zr–0.2Cr–0.3Yb alloy (at.%)

Element	Cr	Yb	Zr	Zn	Mg	Cu	Al
Dispersoid	9.02	3.07	4.59	11.58	3.15	11.67	56.92
α(Al) matrix	0.24	0.04	0.13	3.45	2.41	0.75	92.98

rior. Grain boundaries with continuous η precipitates susceptive to anodic dissolution become the channel for IGC, EXCO and SCC.

As mentioned above, complex additions of Cr, Yb and Zr to Al–Zn–Mg–Cu alloy can remarkably inhibit the recrystallization of Al matrix during solution heat treatment and enhance the resistance to stress corrosion cracking, intergranular and exfoliation corrosion at T6 temper. The effects of complex additions of Cr, Yb and Zr result from the formation of 20–50 nm $(Zr,Yb)Cr_2(Al, Zr, Zn, Mg, Cu)_{20}$ dispersiods in the alloy. The fine dispersiods in AlZnMgCu–0.16Zr–0.2Cr–0.3Yb alloy can stabilize the deformation–recovery microstructure with low angle subgrain or grain boundaries (Fig. 4c and d) by pinning the subgrain boundaries and retarding the transformation of subgrain boundaries to high angle grain boundaries (Fig. 8b). Since the energy of the low angle grain boundaries is much lower than that of the high angle grain boundaries and closer to that of grain interior, the concentration of η precipitates at the low angle grain boundary is lower and more discontinuously distributed. As shown in Fig. 8b, η phase particles are discontinuously distributed at the grain boundaries of the unrecrystallized AlZnMgCu–0.16Zr–0.2Cr–0.3Yb alloy with high proportion of low angle grain boundaries. The discrete distribution of η phase particles at the low angle grain boundaries and the gentle difference of electrochemical property between the low angle grain boundary area and the grain interiorreleave anodic dissolution along grain boundary, result in the improvement of resistance to IGC, exfoliation corrosion and SCC (Figs. 1 and 2 and Table 3) [16].

5. Conclusions

(1) 20–50 nm dispersoids of Zn, Mg, Cu, Zr-containing $YbCr_2A1_{20}$ with cubic $CeCr_2Al_{20}$ crystal structure are formed in Al matrix by complex additions of Yb, Cr and Zr to Al–Zn–Mg–Cu alloy.
(2) Complex additions of Yb, Cr and Zr to Al–Zn–Mg–Cu alloy can remarkably enhance the resistance to recrystallization and stabilize the deformation–recovery microstructure with low angle subgrain or grain boundaries. η phase particles are discontinuously distributed at the grain boundaries of the unrecrystallized AlZnMgCu–0.16Zr–0.2Cr–0.3Yb alloy.

(3) Complex additions of Yb, Cr and Zr to Al–Zn–Mg–Cu alloy can improve the strength, ductility, fracture toughness.
(4) Complex additions of Yb, Cr and Zr to Al–Zn–Mg–Cu alloy can remarkably enhance resistance to stress corrosion cracking (K_{ISCC}) from 9.8 to 17.0 MPa $m^{1/2}$, exfoliation corrosion from EB+ to EA and intergranular corrosion.

Acknowledgements

The authors wish to acknowledge the financial support of National Basic Research Program of China (No. 2005CB623704), National Natural Science Foundation of China (Grant No. 50471057) and Creative research group of National Natural Science Foundation of China (Grant No. 50721003).

References

[1] T.S. Jame, L. John, H.H. Warren Jr., Adv. Mater. Process. 152 (1997) 17–20.
[2] A.L. David, M.H. Ray, Adv. Mater. Process. 10 (1991) 46–49.
[3] J.D. Robson, P.B. Prangnell, Mater. Sci. Technol. 18 (2002) 607–614, 8.
[4] J.D. Robson, P.B. Prangnell, Acta Mater. 49 (2001) 599–613.
[5] D.W. Suh, S.Y. Lee, K.H. Lee, S.K. Lim, H.O. Kyu, J. Mater. Process. Technol. 155–156 (2004) 1330–1336.
[6] Y.L. Wu, F.H. Froes, C.G. Li, A. Alvearez, Metall. Mater. Trans. 30A (1999) 1017–1024.
[7] V.G. Davydov, T.D. Rostova, V.V. Zakharov, Y.A. Filatov, V.I. Yelagin, Mater. Sci. Eng. A 280 (2000) 30–36.
[8] X.Y. Dai, C.Q. Xia, Z.Q. Sun, M.Y. Hua, Y. Wu, Chin. J. Nonferrous Met. 17 (2007) 396–401.
[9] Y.D. He, X.M. Zhang, J.H. You, Trans. Nonferrous Met. Soc. China 16 (2006) 1228–1235.
[10] K.H. Chen, H.C. Fang, Z. Zhang, L.P. Huang, Mater. Sci. Forum 546–549 (2007) 1021–1026.
[11] GB12445.1-90, High Strength Alloys—Method of Stress Corrosion Test for Double Cantilever Beam (DCB) Specimens, National Standard of China.
[12] GB5455-90, The Method for Determining Exfoliation Corrosion of Aluminum Alloys, Aviation Industry Standard of China.
[13] GB7998-87, The Method for Determining the Intergranular Corrosion of Aluminum Alloy, National Standard of China.
[14] S. Niemann, W. Jeitschko, J. Solid State Chem. 114 (1995) 337–341.
[15] F.S. Pan, S.Z. Zhou, P.D. Ding, K. Han, X.F Lin, J. Rare Earths 13 (1995) 21–26.
[16] N. Ruym, B. Haegland, T. Lindveit, Zeit Metalkunde 58 (1967) 28–32.